JOURNAL OF MATERIALS SCIENCE 13 (1978) 483–491

Dislocations and stacking fault energy in silicon ditelluride

P. GRIGORIADIS, J. STOEMENOS
Department of Physics, University of Thessaloniki, Greece

The stacking fault energy in silicon ditelluride single crystals has been determined for different dislocation configurations observed by electron microscopy. The configurations studied are dislocation ribbons and dislocation nodes, and the ratio of the stacking fault energy to the shear modulus is estimated as $\gamma/\mu = 1.6 \times 10^{-11}$ cm. Some common features observed in electron microscopy are also discussed in terms of dislocation networks of extended and contracted nodes and symmetrical or asymmetrical three-fold ribbons, as well as various dislocation interactions.

1. Introduction

$SiTe_2$ is a semiconductor with a layered structure useful for the study of the alloys formed between Si–CdTe interfaces of Si-vidicon targets [2]. There is also considerable interest in structure in connection with polytypism, superstructure, and the existence of short-range order transition states [2, 3].

The present work is concerned with dislocations and stacking faults of the basic structure of $SiTe_2$, which was studied by Weiss *et al.* [4]. It was found to have the hexagonal D^3_{3d}, cadmium iodide-like structure [5], composed of layers of atoms along the hexagonal axis characteristic of cubic close-packing, and in the order

$$\text{–Te–Si–Te–Te–Si–Te–}$$
$$\text{a } \beta \text{ c a } \beta \text{ c}$$

The close-packed layers of Si atoms are sandwiched between two close-packed tellurium layers. The binding between Si and Te is probably stronger than the van der Waals binding between the two tellurium layers. This description refers to the basic structure [4] with $a_0 = 4.28$ Å, $c_0 = 7.71$ Å.

Additional weak diffraction spots reveal a superstructure with a unit cell three times larger than the basic one with $a' = a_0\sqrt{3} = 7.428$ Å and $c' = c_0 = 6.733$ Å. According to Taketochi *et al.* [2] this superstructure may be attributed to a small displacement of Te atoms, Fig. 1, where arrows show the direction of a displacement which differs by about 1.6% of the lattice spacing from the normal position.

Using an automated Philips PW 1100 single crystal diffractometer we were able to establish a unit cell with $a = 7.428$ Å, $c = 13.471 = 2 \times 6.735$ Å, which indicates that $SiTe_2$ appeared with a c-parameter twice the height of the basic structure. This is evidence of the existence of a 4H modification of the compound. It is well known that the most abundant structure of CdI_2 is the 4H polytypic modification [6]. Reflection electron diffraction patterns revealed a two dimensional lattice, disordered parallel to the c-axis, showing different orderings of the stacking sequence [2].

2. Specimen preparation

Single crystals of $SiTe_2$ were grown by following the method described by Rau *et al.* [1]. Stoichiometric amounts of Si and Te were placed in a quartz ampoule, evacuated to 10^{-4} torr and heated for 72 h at 1075° C in a furnace with a small temperature gradient. The ampoule was then slowly cooled. Samples for electron microscopy were easily prepared by cleaving, probably between the tellurium layers where the binding is weak. Specimens from these crystals showed weak extra diffraction spots Fig. 2a, revealing a superstructure formation, although in some cases diffuse scattered intensities appeared, Fig. 2b, which may be attributed to thermal vibration, size

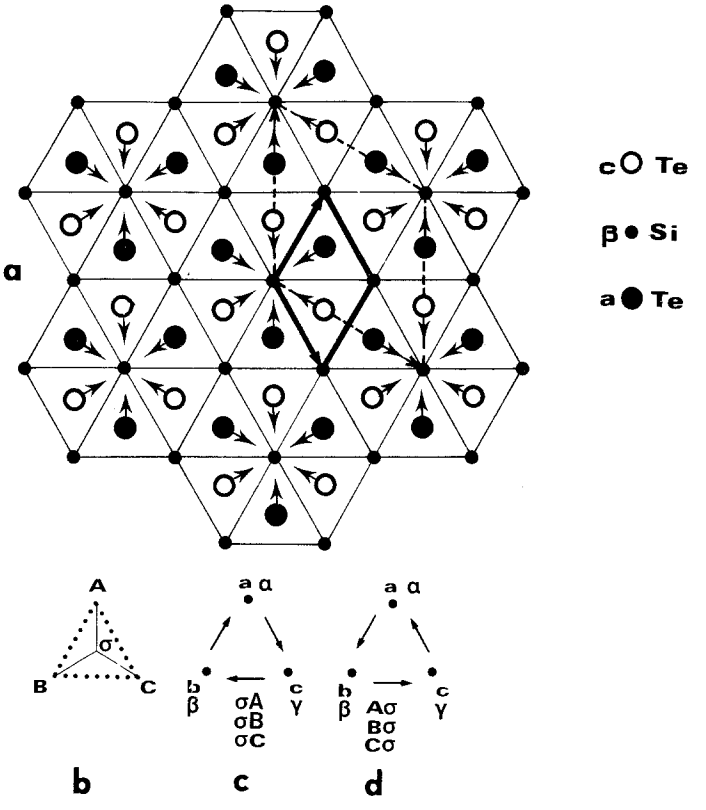

Figure 1 (a) One sandwich of the octahedral structure of silicon ditelluride with indication of the basic (heavy lines) and superstructure (broken lines) unit cell. Arrows show the direction of Te displacements; the Te atoms are on the planes $z = \pm 0.265$ and the Si atoms on the plane $z = 0$. (b) Key for denoting Burgers vectors and (c), (d) the passage of partials with indicated Burgers vectors cause the lettering permutation in the sense of the arrows.

effects or a short-range order amendment. Chemical analysis of the crystals showed a composition range from $SiTe_{1.999}$ to $SiTe_{1.908}$.

In order to avoid superstructure formation, crystals were prepared by a modified method. A sealed ampoule was heated for 72 h at 1100° C in a vertical furnace without a gradient, annealed for 24 h at 900° C and then rapidly quenched in iced water. In this case, the material was mainly polycrystalline, although small single crystals were found suitable for TEM observations. Electron diffraction patterns from these areas revealed that no extra spots were evident, Fig. 2c. Obviously, due to the quenching process from the high temperature, the superstructure could not be formed.

3. Stacking faults

The theoretical considerations for the possible stacking faults in cadmium iodide-like structures have already been given by Siems *et al.* [7]. There are two possibilities. In the first case, a stacking fault results from the wrong stacking of perfect

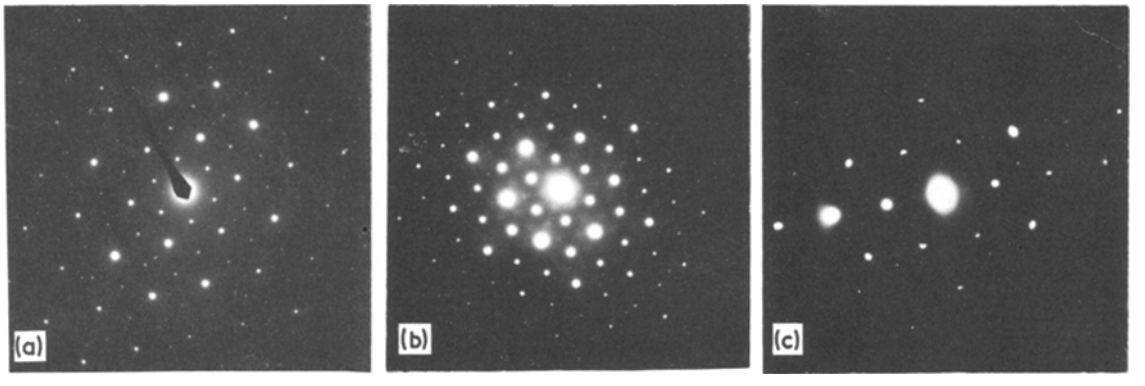

Figure 2 Diffraction patterns from (0 0 0 1) section. (a) Superstructure spots are present which in (c) are absent and in (b) diffuse scattering appears.

sandwiches. A sandwich is called perfect when the atoms in all three of its constituent planes are in different positions. Excluding the possibility of like atom-on-atom stacking, the following stacking sequences are then possible stacking faults

$$a\beta cb\gamma a$$

$$a\beta ca\gamma b$$

$$a\beta cb\gamma c.$$

In the second case stacking faults containing imperfect sandwiches are formed where the atoms in two of its planes are on top of each other. The atom-on-atom planes may be the two Te planes ($a\beta a$) or one Si and one Te plane ($a\alpha b$) The stacking faults of the second type probably have a higher energy than those of the first type because the bonds now are not of the weak van der Waals type.

In the case of CdI_2 or SnS_2 the metallic atoms could occupy only octahedral sites, so the stacking ($a\alpha b$) is energetically very unfavourable and is accompanied by a synchro-shear changing of the sequence from $a\alpha b$ to $a\gamma b$. In the case of $SiTe_2$ the ionic radii are $R(Te^{2-}) = 2.11$ Å and $R(Si^{4+}) = 0.42$ Å [8], so the radius ratio is

$$\frac{R(Si^{4+})}{R(Te^{2-})} = 0.20$$

If in the three stackings $a\beta c$, $a\beta a$, $a\alpha b$ the Te^{2-} spheres of radius R are packed in contact, the radii which the cation spheres should have, to bring them into contact with the anions, are:

For prismatic trigonal $a\beta a$: $0.53R$

For octahedral $a\beta c$: $0.41R$

For tetrahedral $a\alpha b$: $0.22R$

The radius ratio of $SiTe_2$ suggests that the cation can be accommodated in the terrahedral configuration, so that the stacking $a\alpha b$ has not a prohibitive high energy and can occur without the synchro-shear necessary in the case of CdI_2 or SnS_2.

A perfect dislocation in the basal plane of a $SiTe_2$ crystal can dissociate into two Shockley partial dislocations, bounding a stacking fault, according to the schemes

$$AB \longrightarrow A\sigma + \sigma B \quad \text{type I}$$

or

$$AB \longrightarrow \sigma B + A\sigma \quad \text{type II}$$

The possible stacking faults will depend both on the type of separation and on the exact position of the glide plane. Let the normal stacking be $a\beta ca\beta c$ throughout the crystal. Then the possible stacking faults of a dislocation ribbon will be:

type I	$a\beta c/b\gamma ab\gamma a$	(i)
	$a\beta ca/\gamma ab\gamma a$	(ii)
	$a\beta ca\beta/ab\gamma a$	
type II	$a\beta c/c\alpha bc\alpha b$	(iii)
	$a\beta ca/\alpha bc\alpha b$	(iv)
	$a\beta ca\beta/bc\alpha b$	

The slanting line indicates the position of the glide plane.

Thus, from the six possible stacking faults the fault (i) will have the lower energy because it corresponds to the wrong stacking of perfect sandwiches, which remain unsheared. The faults (ii) have one layer of cations in the prismatic trigonal interstices and are expected to have high energy. The fault (iii) has like atoms on top of each other and will have prohibitive high energy, while the faults (iv) have one cation layer in the tetrahedral interstices and will have medium energy.

4. Observations

Observations were made on both types of crystals i.e. with and without superstructure. All crystals showed extensive dislocation configurations. The dislocations were presumably introduced during growth and it is characteristic that crystals without the superstructure formation showed a higher density of dislocations, probably because of the quenching process.

Most of the dislocations were dissociated into partial dislocations. The main glide plane coincides

TABLE I Values of **g.b** for partial dislocations, [0001] orientation

g	**b** = $\frac{1}{3}[10\bar{1}0]$	**b** = $\frac{1}{3}[\bar{1}100]$	**b** = $\frac{1}{3}[0\bar{1}10]$
$20\bar{2}0$	4/3	−2/3	−2/3
$\bar{2}200$	−2/3	4/3	−2/3
$0\bar{2}20$	−2/3	−2/3	4/3
$2\bar{1}\bar{1}0$	1	−1	0
$\bar{1}2\bar{1}0$	0	1	−1
$\bar{1}\bar{1}20$	−1	0	1

with the basal plane which is also the cleavage plane. The lowest stacking fault energy will occur for faults with the glide plane lying between two tellurium layers not containing a silicon atom.

Table I gives values of **g.b** near [0001] orientation. One can see from the table that partials go out of the contrast for reflections of the $11\bar{2}0$ type. However there is a reflection of this type parallel to the total Burgers vector of the ribbon where the two partials will be both visible, Fig. 3, and this is used to determine the total Burgers vector of the ribbon. Dislocation ribbons were very common and the stacking fault energy γ, or rather the quantity γ/μ, was calculated from the variation of the ribbon width as well as from extended dislocation nodes.

4.1. Stacking fault energy

The dependence of the dislocation ribbon width d on its character i.e. the angle α between its total Burgers vector and the dislocation line, is represented [9] by:

$$d = d_0\left(1 - \frac{2\nu}{2-\nu}\cos 2\alpha\right) \qquad (1)$$

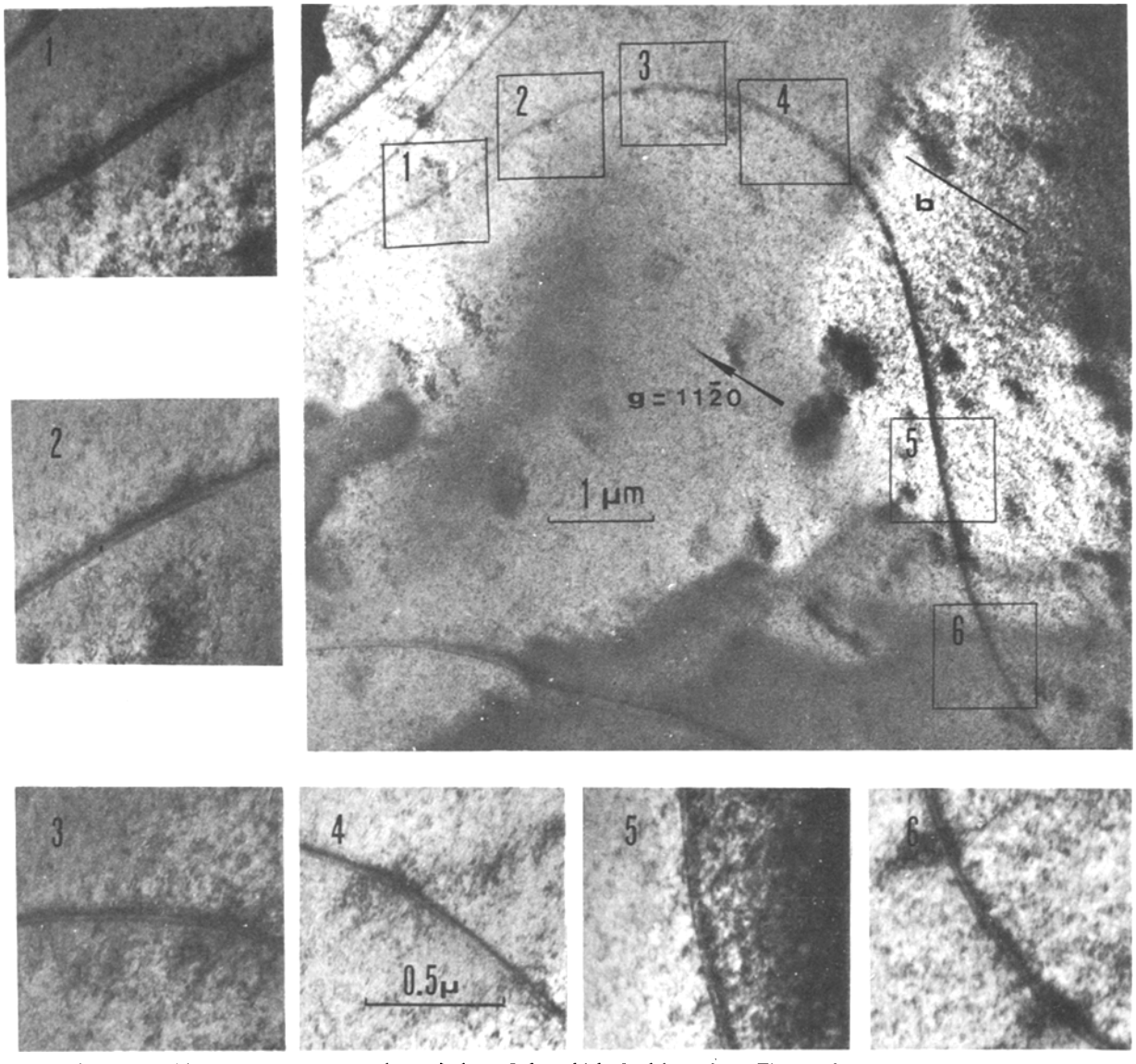

Figure 3 Curved ribbon used to measure the variation of the width d with angle α. The total Burgers vector **b** of the ribbon is also indicated. The insets are segments of the dislocation, all at the same magnification.

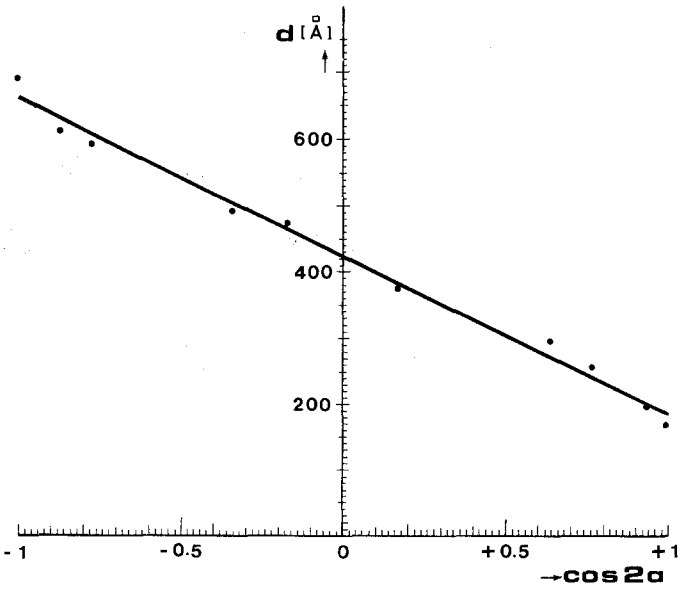

Figure 4 Variation of ribbon width d with $\cos 2\alpha$. A few isolated measurements are also included as data and the least squares fit straight line is indicated.

where

$$d_0 = \frac{\mu \mathbf{b}^2}{8\pi\gamma} \cdot \frac{2-\nu}{1-\nu}$$

and μ is the shear modulus, ν is the Poisson's ratio, γ is the stacking fault energy and **b** is the Burgers vector of the partial dislocation.

Fig. 3 shows one of the ribbons used to measure the variation of the ribbon width as a function of its character, while the insets, which are all of the same magnification, are the different segments used for the measurements. Fig. 4 shows a diagram with the data for this ribbon. The value of ν, deduced from the slope of the straight line, is $\nu = 0.43 \pm 0.05$, while $d_0 = 430$ Å.

Using these values and $\mathbf{b} = 2.47$ Å for $SiTe_2$, the value $\gamma/\mu = 1.6 \times 10^{-11}$ cm could be derived. All experimental errors were carefully controlled [10]. Calculations of intensity profiles of the ribbon used were performed in order to investigate the effect of the dislocation image shift on the stacking fault energy measurements. The calculations were based on the two-beam dynamical equations of electron diffraction including absorption. Microdensitometer traces of all the different segments of a curved ribbon were taken with an output magnification of 50 × and the apparent ribbon widths were measured. These widths were considered to correspond to the "true" partial dislocation distances of the ribbon. The intensity profiles of all the segments were then calculated and were found to give apparent, i.e. peak-to-peak, partial dislocation distances about 1% greater than the used "true" distances for the calculations. Hence the value of the stacking fault energy should be increased by 1% which is well within the error of measurement.

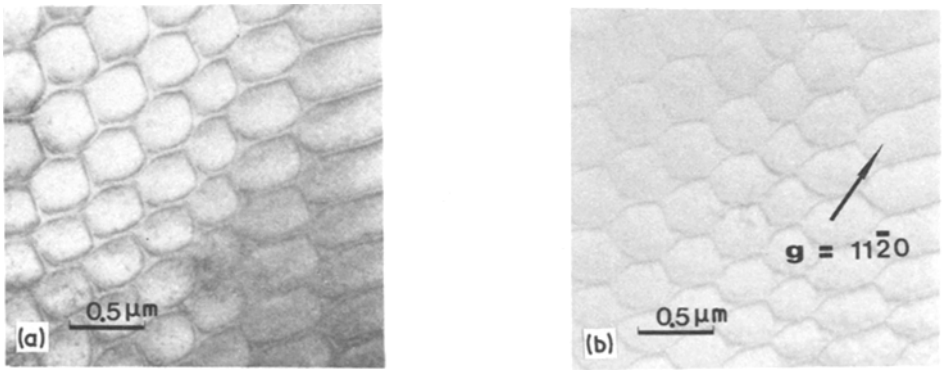

Figure 5 (a) Network of extended and contracted dislocation nodes. (b) The same area with one set of partial dislocations out of contrast.

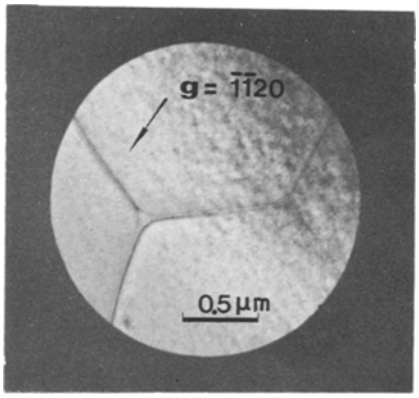

Figure 6 Interaction of two isolated dislocation ribbons and the formation of extended and contracted nodes.

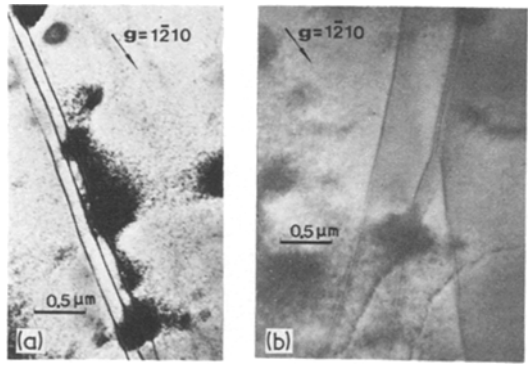

Figure 7 (a) Symmetrical and (b) asymmetrical three-fold ribbons.

The calculations involved together with the computer program have been the subject of a paper by one of us [11].

Fig. 5a shows an array of extended and contracted nodes. One set of partial dislocations is out of contrast in Fig. 5b. The mean value of the node width $w = 500$ Å; the radius of curvature $\rho = 1600$ Å and the node character $\alpha = 40°$ were measured from Fig. 5a.

The equilibrium configuration of extended dislocation nodes was studied by Brown [12, 13], Siems [14] and Jossang *et al.* [15]. Following the theory of Brown and taking $\nu = 0.43$ and $\mathbf{b} = 2.47$ we have calculated the values $\gamma w/\mu \mathbf{b}^2 = 0.29$ and $\gamma/\mu = 3.5 \times 10^{-11}$ cm. This value of γ/μ is larger than the value found by the ribbon width method. However, the radius of node curvature is large compared to the foil thickness and the assumption of infinite medium becomes a poor approximation [13]. Thus, the results of the above two methods are comparable within their limitations, and give the order of magnitude of the stacking fault energy for the low energy stacking faults.

Fig. 6 shows the reaction of two isolated ribbons and the formation of an extended and a contracted node. The value of γ/μ deduced from the extended node is the same as the value obtained using the extended nodes of the network in Fig. 5a. No difference was found in the stacking fault energy between crystals with and without superstructure, within the limits of the experimental error.

4.2. Three-fold ribbons

Symmetrical as well as asymmetrical three-fold ribbons have been observed, Figs. 7a and b. Symmetrical three-fold ribbons could be produced by the following reaction

$$(A\sigma + \sigma B) + (\sigma C + A\sigma) \longrightarrow A\sigma + A\sigma + A\sigma$$

type I type II

i.e. the two innermost dislocations combine and no overlapping occurs [7].

This is evidence that type II stacking faults do exist and also that the two stacking faults have roughly equal energy. The width w of the symmetrical three-fold ribbon is a function of its character [10] i.e.

$$w = w_0 [1 - (\nu/2 - \nu) \cos 2\alpha] \qquad (2)$$

where

$$w_0 = \frac{3\mu \mathbf{b}^2}{4\pi\gamma} \cdot \frac{2-\nu}{1-\nu}$$

The width d of a single ribbon is also a function of its character (Equation 1) and for the same value of $p = \cos 2\alpha$ the ratio w/d is a function of ν given by

$$\frac{w}{d} = \frac{6[2 - \nu(1+p)]}{2 - \nu(1+2p)}$$

In Fig. 8 the ratio w/d is plotted as a function of ν. The measured width of the three-fold ribbon in Fig. 7a is $w = 2400$ Å and its character is $\alpha = 40°$. The corresponding value of a single ribbon for $\alpha = 40°$ is $d = 380$ Å, Fig. 4, so that the ratio w/d becomes equal to 6.32. From Fig. 8 the deduced value of ν is $\nu = 0.44$, which is in good agreement with the previously calculated value $\nu = 0.43$.

Asymmetrical three-fold ribbons (Fig 7b) could be produced by a cross-over reaction of two simple ribbons of the same type, when overlapping takes

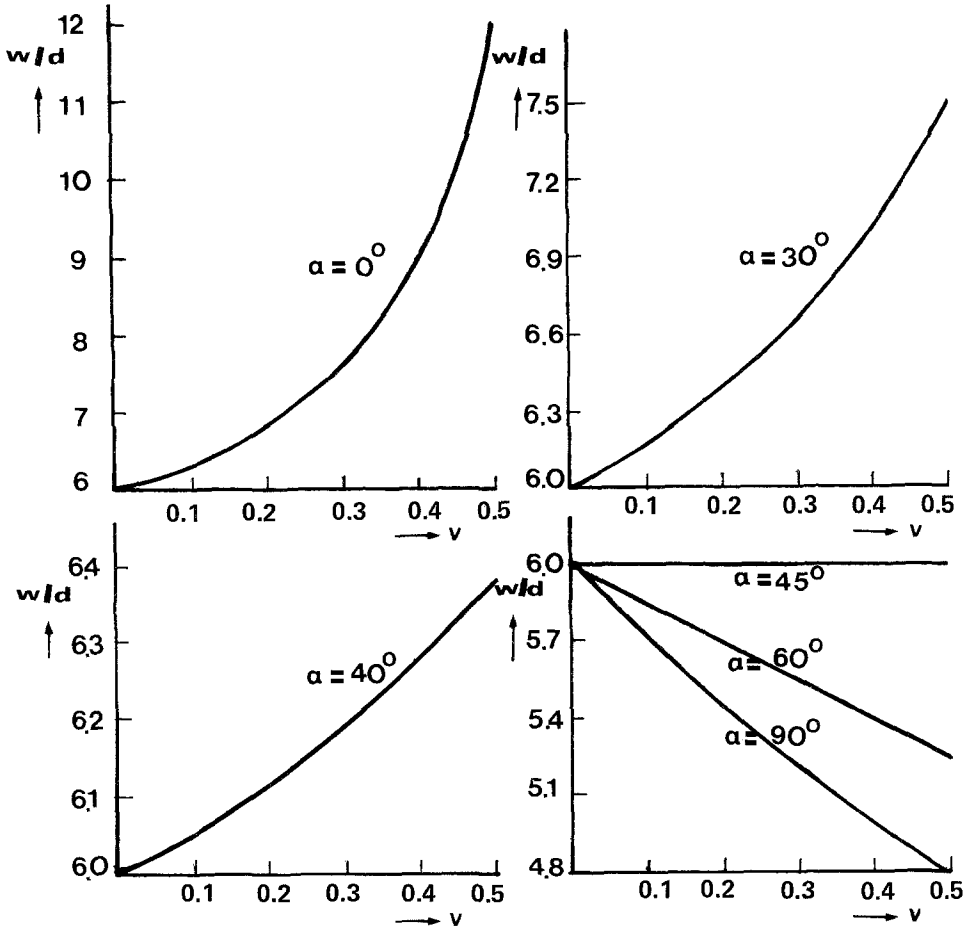

Figure 8 Plot of the variation of w/d as a function of ν for various angles α.

place. A possible reaction could be of the form

$$(A\sigma + \sigma B) + (A\sigma + \sigma C) = A\sigma + A\sigma + A\sigma$$

type I type I

The ratio of the stacking fault energies in both regions can be determined from the width of the two halves by means of the formula [7];

$$\frac{\gamma_1}{\gamma_2} = \frac{r(2+r)}{2r+1}$$

where r is the ratio of the widths. The measured value of r is 2.4 which gives $\gamma_1/\gamma_2 = 1.8$. This is very close to the theoretical value $\gamma_1/\gamma_2 = 2$ for overlapping faults of the same type (I or II).

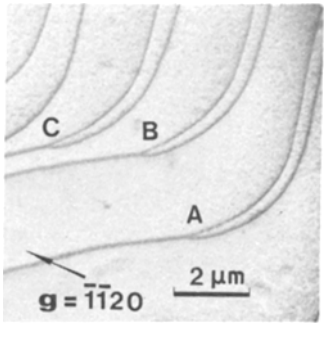

Figure 9 Undissociated dislocations repel each other upon changing their direction.

4.3. Interaction of dislocations

Regular networks were commonly observed. The interaction of ribbons in the same glide plane leads to the formation of a hexagonal network of extended and contracted nodes, Fig. 5a.

Perfect dislocations in the basal plane were also observed, Fig. 9. Probably the stacking fault energy is so large that no visible dissociation occurs. Some of the undissociated dislocations seem to dissociate upon changing their orientations at A, B, C. A possible explanation [10]

could be that these are, in fact, two dislocations in edge orientation one on top of the other in an equilibrium position. Upon changing direction they become screw dislocations and as a consequence they repel each other.

The dislocation in Fig. 10a has dissociated into partials at A, B, C, making a sequence of loops. In Fig. 10b both partials are visible while in Fig. 10c one partial is out of contrast for an operating reflection of $11\bar{2}0$ type. The Burgers vectors of the partials were of the $a/3$ $\langle 10\bar{1}0 \rangle$ type. A possible interpretation for this reaction is an interaction between the dislocation and a sequence of loops [16]. A strong interaction between the dislocation and the loop requires the loop to have a Burgers vector component in the basal plane. Nevertheless, no isolated loops have been observed, which indicates that the origin of these loops is closely related to the dislocations. The case for the loops to be interstitial, with Burgers vectors perpendicular to the basal plane, is very unfavourable. This is because basal plane dislocations interact with inerstitial loops only through their long-range stress fields and it is unfavourable energetically to produce any splitting into partials. Furthermore, we have not observed the characteristic residual contrast of the isolated interstitial loops and tilting the specimen at about 25° has not revealed loops of this type.

5. Conclusions

The ratio γ/μ for $SiTe_2$ was found to be 5 times larger than that for SnS_2 while the order of magnitude of the width of the dislocation ribbons for $SiTe_2$ was about 5 times smaller than that for SnS_2, which has the same structure. These may suggest that the stacking fault energy of $SiTe_2$ is rather high for a layered structure crystal. The stacking faults of dislocation ribbons were analysed in Section 3.

The occurrence of fault (iii) is improbable because of its high energy, while fault (iv) is not unfavourable in our case as it was concluded in Section 3 that a synchro-shear movement should not be expected. Case (i) produces the lowest energy deviation from the normal stacking sequence and the calculated value of the γ/μ should be attributed to this case. Moreover, it is unambiguously concluded from the symmetrical three-fold ribbons that the low energy (typeII) stacking fault (iv) can occur.

The phenomenon of polytypism is closely related to the stacking fault energy and from this point of view the $SiTe_2$ is appropriate for electron microscopy observations unlike CdI_2 which decomposes when exposed to normal electron beams [6], and consequently no experimental value for stacking fault energy has been available for this compound until now.

6. Acknowledgements

It is our pleasure to acknowledge the stimulating discussions with Professor N. A. Economou and Dr J. Antonopoulos. We would also like to thank Professor K. Alexiadis, director of the laboratory of Analytical Chemistry of the Chemical Engineering Department and Professor G. Vassilikiotis, director of the Laboratory of Analytical Chemistry of the School of Physics and Mathematics, for the chemical analysis of the crystals. Also thanks are due to Dr A. Lambros and Mr K.

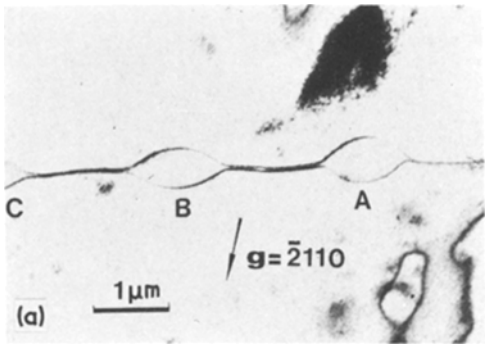

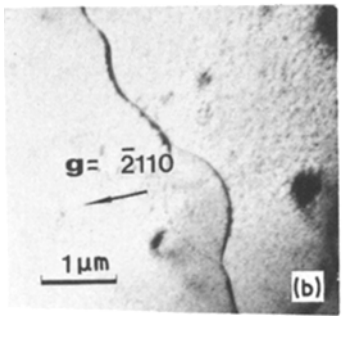

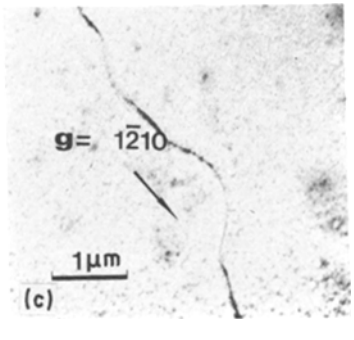

Figure 10 (a) interaction between a dislocation and a sequence of loops; (b) both sides of the loop are in contrast and in (c) one side of the loop is out of contrast.

Paraskevopoulos for providing the crystals, and to Dr S. Kokou for his help with the diffractometer measurements.

References

1. J. W. RAU and C. R. KANNEWURF, *J. Phys. Chem. Solids* **27** (1966) 1097.
2. K. TAKETOSHI, S. YOSHIKAWA and K. HAMANO, *NHK Tech. J.* (Japan), **26** (1974) 172.
3. A. P. LAMBROS and N. A. ECONOMOU, *Phys. Stat. Sol. (b)* **57** (1973) 793.
4. A. WEISS and A. WEISS, *Z. Annorg. Chem.* **273** (1953) 124.
5. R. W. G. WYCKOFF, "Crystal Structures" Vol. 1 Intersciences, New York, (1968) p.269.
6. R. PRASAD, *Phys. Stat. Sol. (a)* **38** (1976) 11.
7. R. SIEMS, P. DELAVIGNETTE and S. AMELINCKX, *Phil. Mag.* **9** (1964) 121.
8. "Handbook of Chemistry and Physics", 47th edition, edited by R. C. Weast (The Chemical Rubber Co., 1966)
9. W. T. READ, "Dislocations in Crystals", (McGraw-Hill, New York, 1953) p.131.
10. S. AMELINCKX and P. DELAVIGNETTE, "Electron Microscopy and Strength of Crystals", edited by G. Thomas and J. Washburn (Intersciences, New York, 1963) p. 441.
11. P. GRIGORIADIS, *Sci. Annals, Fac. Phys. Mathem. Univ. Thessaloniki* **16** (1976) p. 441.
12. L. M. BROWN and A. R. THÖLEN, *Trans. Faraday Soc.* **38** (1964) 35.
13. L. M. BROWN, *Phil. Mag.* **10** (1964) 441.
14. R. SIEMS, *Disc. Faraday Soc.* **38** (1964) 42.
15. T. JOSSANG, M. J. STOWELL and J. P. HIRTH, *Acta Met.* **13** (1965) 279.
16. G. K. WILLIAMSON and C. BAKER, *Phil. Mag.* **6** (1961) 313.

Received 21 March and accepted 25 July 1977.